Energy Reports 7 (2021) 4222–4234

Contents lists available at ScienceDirect

Energy Reports

journal homepage: www.elsevier.com/locate/egyr

Research paper

Ultra-stable nanofluid containing Functionalized-Carbon Dots for heat transfer enhancement in Water/Ethylene glycol systems: Experimental and DFT studies

Saeed Askari [a,b], Ehsanollah Ettefaghi [a,c], Alimorad Rashidi [a,*], Abdolvahab Seif [a,d], Jennifer A. Rudd [e], Julio A. Alonso [d], Saeed Khodabakhshi [e]

[a] Nanotechnology Research Center, Research Institute of Petroleum Industry (RIPI), West Blvd. Azadi Sports Complex, P.O. Box 14665, 1998, Tehran, Iran
[b] Department of Chemical and Biomolecular Engineering, National University of Singapore, P.O. Box 117585, Singapore
[c] Department of Mechanical & Biosystems Engineering, Tarbiat Modares University, P.O. Box 14115-336, Tehran, Iran
[d] Departamento de Física Teórica, Atómica y Óptica, Universidad de Valladolid, 47011 Valladolid, Spain
[e] Energy Safety Research Institute, Swansea University, Bay Campus, Swansea, SA1 8EN, UK

ARTICLE INFO

Article history:
Received 17 March 2021
Received in revised form 12 June 2021
Accepted 2 July 2021
Available online xxxx

Keywords:
Functionalized-carbon dots
Ultra-stable nanofluid
Heat transfer
Thermo-physical properties
DFT

ABSTRACT

A facile hydrothermal method was applied to synthesize functionalized-carbon dot nanoparticles. The analysis revealed a low crystallinity with amorphous nature for particles with a size below 17 nm, which were functionalized with oxygen (17.9%) and nitrogen (12.2%). A nanofluid was formed by dispersing the nanoparticles in a mixture of water and ethylene glycol. The zeta potential measurement confirmed the stability of the nanofluid (-61.5 mV). Viscosity and density measurements revealed that the suspended nanoparticles did not noticeably increase the viscosity (maximum 8%) and density (maximum 1.2%). The thermal conductivity increased as temperature and nanoparticle concentration increased, and a maximum enhancement of 21% was obtained at 45 °C and 0.5 Wt%. Then, the convection heat transfer was investigated in the turbulent regime. The results showed a remarkable enhancement of the convective heat transfer coefficient (34%) at the Reynolds number of 15529 and 0.5 Wt%. Finally, the density functional theory (DFT) method was applied to interpret the long-term stability of the nanofluid. These results showed that the surface functional groups play a prominent role in the stability of the nanofluids. The calculations indicate that the bonding between the functionalized nanoparticles and the solvent fluid occurs through hydrogen bonds and electrostatic dipolar interactions.

1. Introduction

One of the biggest challenges facing the world today is the production and distribution of energy. In this regard, heat transfer is an inseparable part of many industrial processes which employ a flowing fluid in a wide range of pressures and temperatures (Borode et al., 2019). Decreasing the thermal resistance of fluids is favorable for many applications because it helps to produce smaller heat transfer devices, and leads to lower cost, and more energy-efficient systems (Sözen et al., 2021). To date, nanofluids are a promising candidate to reduce thermal resistance, and various industrial applications can benefit from their outstanding characteristics (Qeays et al., 2020; Gupta et al., 2018). Dispersing nanoparticles in base fluids such as water, ethylene glycol (EG), and oil can enhance the thermal properties of the base fluids (Li et al., 2020a). As the nanoparticles thermal conductivity is significantly higher than that of the base fluids, suspending nanoparticles in a base fluid, even at low concentration, can have a strong impact on enhancing thermal performance (Ambreen and Kim, 2020). In this regard, many investigations have been done on different aspects of nanofluids. All these investigations have reported that nanofluids have special properties, which are generally different from those of conventional heat transfer fluids. As will be discussed subsequently, much research has been conducted on the effect of metal-based and carbon-based nanoparticles to enhance heat transfer characteristics in various types of conventional fluids. The obtained results showed that typical nanofluids can enhance thermal properties up to 40% depending on the base fluids and the type of nanoparticles employed. Particularly, nanofluids have distinctive features including a significant temperature dependency of the properties (Jiang

* Corresponding author.
E-mail address: Rashidiam@ripi.ir (A. Rashidi).

https://doi.org/10.1016/j.egyr.2021.07.001

Nomenclature

Symbol	Meaning
Z	Entrance length, m
D_i	Inner tube diameter, m
Q''	Heat flux, W/m^2
V	Voltage, V
I	Electrical current, A
K	Thermal conductivity, W/(m K)
μ	Dynamic Viscosity, Pa s
ρ	Density, kg/m^3
E_b	Binding energy, kJ/mol
L	Tube length, m
h	Heat transfer coefficient, W/(m^2 K)
T	Temperature, °C
Ts	Surface temperature, °C
Tm	Average fluid temperature, °C
p	Surface perimeter, m
$\dot{m}$	Mass flow rate, kg/s
Cp	Specific heat capacity, J/(kg K)

et al., 2019), thermal conductivity and heat transfer coefficient enhancement even at low nanoparticle loading (Shdaifat et al., 2020), and critical heat flux (CHF) enhancement in a pool boiling (Mori et al., 2019). Although the heat transfer coefficient is considered as an important parameter in forced-convection applications, the thermal conductivity enhancement is a more reliable indicator of the nanofluid heat transfer enhancement over its base fluid (Jóźwiak et al., 2020). There are theories to explain how dispersed nanoparticles in a base fluid can improve heat transfer properties, such as the Brownian motion theory (Ashraf et al., 2020). Brownian motion is defined as a random motion of nanoparticles, which may shrink the thickness of the thermal boundary layer; this has significant consequences on heat transfer enhancement. In addition, the Brownian motion would result in increasing the slip velocity in the available surface among particles and fluid media (Nojoomizadeh et al., 2018). Although increasing nanoparticles loading may cause a higher heat transfer enhancement, the higher nanoparticle loading results in higher viscosity, which has a negative feedback on increasing pumping power (Sarsam et al., 2015). In addition, the long-term stability of suspended nanoparticles may decrease by increasing its volume fraction (Mukherjee et al., 2018). Addition of surfactants is one of the typical methods to improve the stability in the two-phase systems. Using surfactants can improve nanofluids' stability in a short term, but the main problem is that surfactants cannot guarantee a long term stability and also can adversely affect the thermal conductivity of prepared nanofluids. In this regard, surfactant-free methods including functionalized nanoparticles are highly recommended to prepare ultra-stable nanofluids (Esmaeili et al., 2019) with long-term stability (Karthikeyan et al., 2018). This can open a window to use doped materials (e.g. nitrogen/oxygen-doped carbon nanoparticles) which have been successfully synthesized (Wang et al., 2018; Li et al., 2019).

Moving forward, utilization of nanofluids in industrial cooling and heating systems will cause great energy savings and reduction of carbon emissions. To be more specific, using nanofluids in most typical cooling and heating systems has a potential to save 1 trillion Btu of energy (Wong and De Leon, 2017). For example, it has been reported in the US electric power industry that using nanofluids in closed loop cooling cycles can save energy up to 10–30 trillion Btu per year, which is equal to the amount of energy that 50,000–150,000 households consume in a year (Minkowycz et al., 2016). In addition, from the environmental point of view, using nanofluids can decrease the emission of toxic gases into the atmosphere; approximately, 21,000 tons of SO_2, 8,600 tons of NO_x, and 5.6 million tons of CO_2 (Wong and De Leon, 2017).

Akram et al. investigated carbon and metal based nanofluids in a flat-plate solar collector (Akram et al., 2021). They reported that the thermal conductivity was enhanced by 25.68% for functionalized carbon dot nanofluids compared to the base fluid. Hussein et al. studied the heat transfer performance of GNPs and multiwall carbon nanotube (MWCNT) nanofluids in a flat-plate solar collector, and the results showed that at 0.1wt% the thermal performance of the collector was enhanced by 21.9% (Hussein et al., 2020). Li et al. applied surface modification of MWCNTs to investigate the stability, viscosity, and thermal conductivity of nanofluids (Li et al., 2020b). They reported that a long term stable nanofluid with a maximum thermal conductivity enhancement of 69.68% was achieved at 5wt%. Kazemi et al. studied the thermal conductivity enhancement of a graphene based nanofluid (Kazemi et al., 2020). Their results showed that dispersing graphene in water (1 wt%) can enhance by 41.39% the thermal conductivity compared to the base fluid at 50 °C.

With a view on future industrial scale-up, here, a simple and practical method has been applied to synthesize functionalized-carbon dot (F-CD) nanoparticles. As the stability of the nanoparticles in fluids is an important factor which can limit the nanofluids usage, in the current work, ultra-stable nanofluids have been prepared that remain stable for a long time without any sedimentation and with appropriate thermo-physical properties. Then, we rationalize the long-term stability of suspended nanoparticles in the base fluid by theoretical calculations. We believe that this method can be considered for industrial applications to improve performance, save a great deal of energy, and reduce releasing a huge number of toxic gases into the atmosphere.

2. Experimental section

2.1. Materials

To synthesize the nanoparticles, industrial-grade citric acid ($C_6H_8O_7$) and urea (CH_4N_2O) were purchased from Pardis petrochemical unit, Iran. Distilled water and Ethylene Glycol were used as the solvent.

2.2. Nanoparticle synthesis procedure

6 g of citric acid were added into 40 mL of distilled water and the mixture was stirred at room temperature until a transparent solution was obtained; then, 6 g of urea was added to the solution. A mechanical stirrer was applied to reach a high level of mixing while the temperature was kept at 40 °C until a viscous solution was obtained. After that, the viscous solution was transferred into a cubic furnace and the temperature was increased to 350 °C (heating rate: 5 °C /min) for 3 h under Argon atmosphere.

2.3. Nanofluid preparation

The F-CD nanofluid was made by dispersing nanoparticles in the range of 0.05–0.5 Wt% into a mixture of deionized water and ethylene glycol (7:3 ratio). The ratio of 7:3 was selected because in most industrial applications the ratio of water to ethylene glycol is considered 7 to 3. Considering that the synthesized F-CD nanoparticles were hydrophilic, a simple stirring was applied for 10 min to stabilize the particles in the base fluid. To produce the nanofluids in an industrial scale, a simple mechanical mixer was applied for 10 min to suspend the nanoparticles in the base fluid.

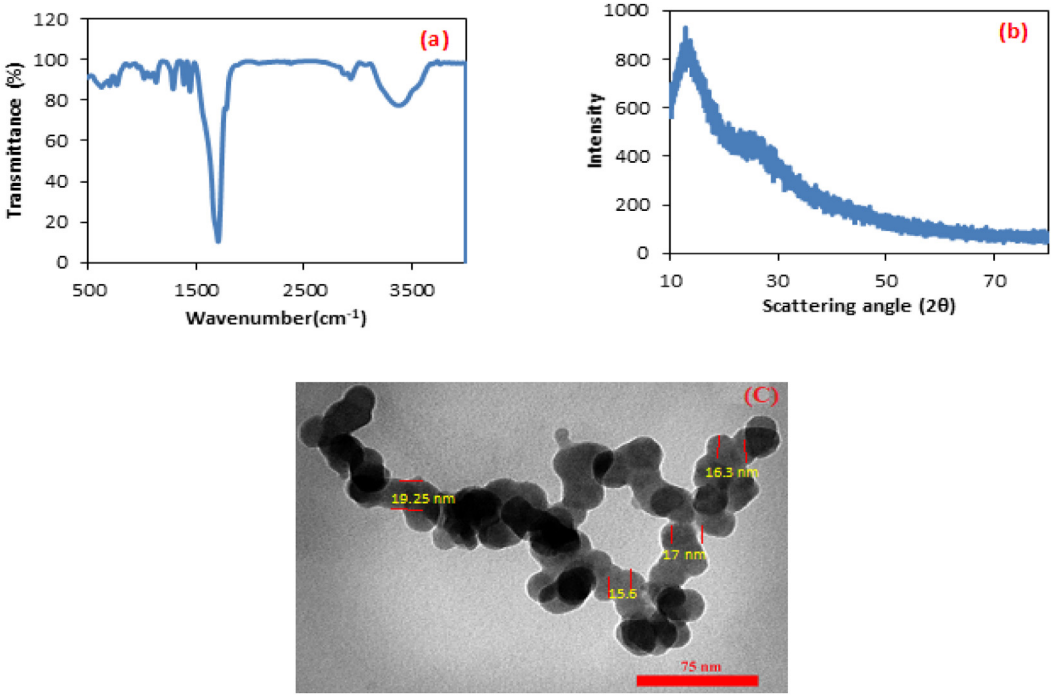

Fig. 1. (a) FTIR spectra, (b) XRD patterns, and (c) TEM image of synthesized F-CDs.

2.4. Experimental setup for convection heat transfer measurement

To measure the convection heat transfer coefficient, an experimental setup was designed, Fig. 1S. The system mainly comprises a copper tube test section (diameter: 10 mm and length: 900 mm) and a shell&tube heat exchanger (14 inside tubes of diameter: 7 mm and length: 580 mm). The flow rate was adjusted in the range of 0.01–0.05 l/s with a pump (HV-77921-40). In the Supporting Information file further description and schematics of the experimental setup can be found.

To calculate the heat transfer coefficient, the following equations, based on surface with constant heat flux, were utilized. The convection heat transfer coefficient is defined in Eq. (1), in which h(z), Q″, $T_a(z)$, and $T_s(z)$ are defined as the heat transfer coefficient, constant surface heat flux, average temperature in bulk fluid, and test section surface temperature, respectively. $T_a(z)$ and Q″ are calculated by Eqs. (2)–(3) (Bazmi et al., 2019).

$$h(z) = \frac{Q''}{T_s(z) - T_a(z)} \tag{1}$$

$$T_a(z) = T_{a,i} + \frac{Q'' p}{\dot{Q} c_p} \tag{2}$$

$$Q'' = \frac{IV}{\pi LD} \tag{3}$$

where in Eq. (2) $T_{a,i}$ is the inlet flow temperature, p is the surface perimeter, $\dot{Q}$ is the flow rate, c_p is the specific heat capacity, and z is the axial distance. In Eq. (3), I stands for electrical current, V stands for voltage, L stands for tube length, and D stands for diameter.

The supplementary file contains all details about the characterization methods and measurement uncertainty of all experimental data (Table.S1, Supporting Information).

3. Results and discussion

3.1. Characterization of Functionalized-Carbon Dots

F-CD nanoparticles were characterized using FTIR, XRD, and TEM as shown in Fig. 1. To study the covalent bonding on F-CDs, the Fourier Transform Infrared Spectrum (FTIR spectra, PerkinElmer Spectrum GX) was measured (Fig. 1a). The presence of C=C bonding is indicated by the signal at frequency position of ∼1571 cm^{-1}. This signal shows the presence of the basic component of graphene (Park et al., 2020). The C=O tensile vibration is observed at the absorption band region of ∼1730 cm^{-1} (Lyu et al., 2020). The wide absorption band in the 2700–3600 cm^{-1} region is due to -OH groups: HO–C=O and C–OH (Ding et al., 2013). Tensile C–N absorptions appeared at ∼1192 cm^{-1}, and also the N–H bending is observed at ∼1540 cm^{-1} (Mondal and Saha, 2019).

The X-ray diffractometer (XRD X'Pert MPD model, Philips, Holland) pattern of F-CDs displayed in Fig. 1b indicates a low crystallinity along with amorphous nature of the synthesized F-CDs. The diffraction peak (002) of bulk graphite is revealed at $2\theta = 26.3°$ with d-spacing of 0.34 nm (Sharma et al., 2019). In addition, the broadness of XRD peaks is related to small size of F-CDs (Zhang et al., 2012). Morphology and crystal size of the synthesized nanoparticles were analyzed by Transmission Electron Microscopy (TEM, a JEOL JEM-2010F microscope operated at an accelerating voltage of 200 kV), Fig. 1c. As seen, uniform spherical particles with a size of ≈17 nm have been synthesized.

Raman spectroscopy is another powerful technique to disclose the particle's structure. Fig. 2 shows the Raman spectrum of the F-CDs; both the D and G bands are revealed at 1338 and 1556 cm^{-1}, respectively. The D band is related to disorder in sp^2 hybridized carbon, and the G band is attributed to first-order scattering of sp^2 carbon domains (Lyu et al., 2020).

The existence of carbon, nitrogen and oxygen in the sample was measured by elemental distribution mapping (Fig. 2S), in which the nitrogen and oxygen are uniformly distributed over the F-CDs structure. This can play an important role in enhancing the material's stability and heat transfer capability.

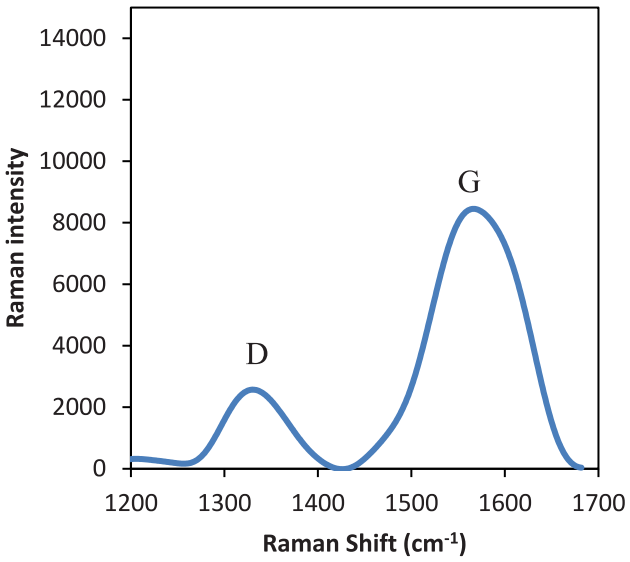

Fig. 2. Raman spectrum of the synthesized F-CDs.

The X ray photoelectron spectroscopy (XPS) analysis of the F-CDs corroborates the findings using elemental distribution mapping, namely that carbon, oxygen and nitrogen are spread evenly across the surface, see Figs. 3 and 4. The material's surface consists of 69.9% carbon, 17.9% oxygen and 12.2% nitrogen. The surface of the material, according to XPS, consists of amine groups and a mixture of aliphatic C–OH groups (29.0% by carbon) and carboxylic O–C=O groups (13.5% by carbon). The breakdown of the relative intensities of the carbon and oxygen component peaks is detailed in Supplementary Material. This observation of the C–OH and O–C=O groups by XPS analysis is in line with the FTIR observations detailed above. The major carbon component corresponds to the overlapping sp^2 and sp^3, C=C and C–C bonded carbon.

3.2. Stability

To evaluate the stability of nanofluids, several methods have been used in the literature, namely UV–visible spectroscopy, Zeta potential, sedimentation photography, and others (Kumar et al., 2019). In this investigation, sedimentation photography and Zeta potential were used to examine the stability of prepared nanofluids over time. In Fig. 3S, the photos of fresh nanofluids are compared with the photos of the prepared nanofluids after a month, three months, and after a year, which were left in a stable vibration-free environment. As can be seen, no sedimentation was observed after a year even at the highest nanoparticle concentration (0.5 Wt%), which confirms the long-term stability of the prepared nanofluids. It should be mentioned that sedimentation photography is not able to completely confirm the stability of nanofluids because of the brown color of the nanofluids. In this regard, the stability of the nanofluids was investigated by Zeta potential measurements; a higher Zeta potential reveals a higher stability of nanofluids. Thus, a nanofluid with high Zeta potential is stabilized electrically, and a fluid with low Zeta potential tends to aggregate. In general, a nanofluid with Zeta potential above ±60 mV is defined as ultra-stable nanofluid (Choudhary et al., 2017). Fig. 5 shows the Zeta potential of the prepared nanofluid at concentration of 0.5 Wt%. It is observed that the Zeta potential value for the fresh sample and for a year-old sample were determined as −61.5 mV and −59.7 mV, respectively. These values show that the prepared nanofluid has an excellent stability even after a year. As discussed previously based on the XPS result, F-CD nanoparticles contain a high level of nitrogen (12.2%) and oxygen (17.9%) which significantly tend to interact with hydrophilic liquids, likely via intermolecular hydrogen bonding, leading to a high stability. Although some researchers used functionalized nanoparticles to improve the stability of nanofluids, the number of functional groups on the nanoparticles surface is still not enough to prevent aggregation as time went by. Thus, in this research, nanoparticles were functionalized during the syntheses process, resulting in a high number of functional groups, which established strong bonds with the surface of the nanoparticles. In most previous publications, nanoparticles were functionalized by a chemical treatment after synthesis, which caused a low number of functional groups and poor bonding, as seen in Table 1. Especially for carbon-based nanofluids, these were stable just for few days.

The stability of the current nanofluid has been compared in Table 1 with the stability period of different nanofluids reported in the literature. As can be seen, in most investigations researchers have not been able to produce a nanofluid with a long-time stability. In the current work, the addition of F-CD nanoparticles has been able to solve this crucial issue even in an industrial scale, which accentuates the value of these particles.

In comparison, most researchers tried to prepare stable nanofluids using surfactants, functionalizing the particles surface, and exposing the system to ultrasonic waves. Although applying these methods may help us to make a nanofluid stable for a short time, these are not efficient ways to produce an ultra-stable nanofluid for a long time. For instance, the usual surface treatments just help to functionalize the nanoparticles surface by physical bonding (physisorption). As the strength of physical bonding is week, the functionalization tends to degrade after a short period of time. In addition, exposure to ultrasonic waves helps to separate aggregated nanoparticles. When the nanoparticles are not aggregated, they can remain stable because aggregated nanoparticles have higher weights, which accelerate their sedimentation. However, after a short period nanoparticles start to aggregate because of van der Waals forces. One of the purposes of the current work has been to prepare hydrophilic nanoparticles by tightly attaching functional groups containing oxygen and nitrogen by a chemical functionalization method during the synthesis process. In comparison with physical functionalization, the chemically functionalized groups establish strong intermolecular bonds with the particles surface. Thus, these functional groups enhance the hydrophilicity of the suspended nanoparticles, which remain stable in the base fluid for a longer period.

3.3. Stability of the nanofluid from density functional calculations viewpoint

Density functional theory (DFT) calculations have been performed to support and interpret some of the experimental results reported above, specifically the long-term stability of the nanofluid. The calculations have been performed with the Gaussian 09 code (Frisch et al., 2010), with a 6–31(d) basis set to expand the electronic molecular orbitals. Electronic exchange and correlation effects are taken into account by the hybrid M06-2X functional (Zhao and Truhlar, 2008). This functional was found to give a good account of noncovalent interactions and the results were reported to be in good agreement with experimental data (Pourreza et al., 2019; Zhao et al., 2006; Sert et al., 2014; Srivastava et al., 2017; Tehrani et al., 2019). To model the aqueous solvent we employed the Conductor-like Polarizable Continuum Model (CPCM), a continuum solvation model which takes into account the interactions between the solute and the solvent,

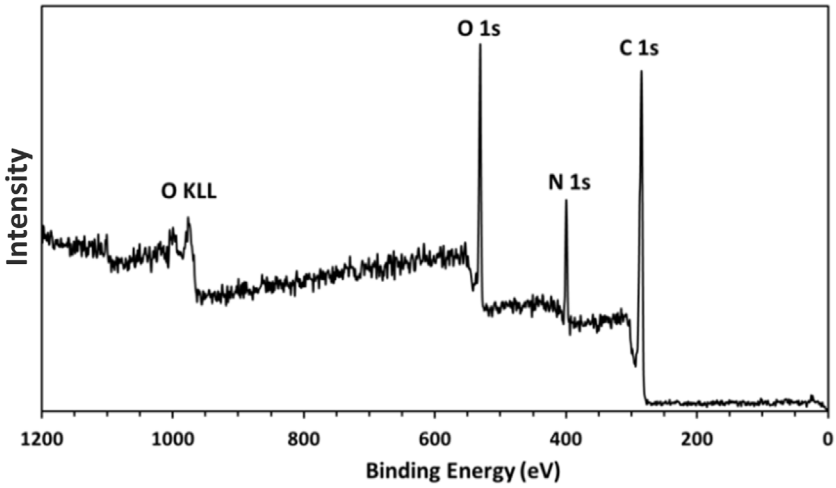

Fig. 3. XPS spectrum of F-CDs.

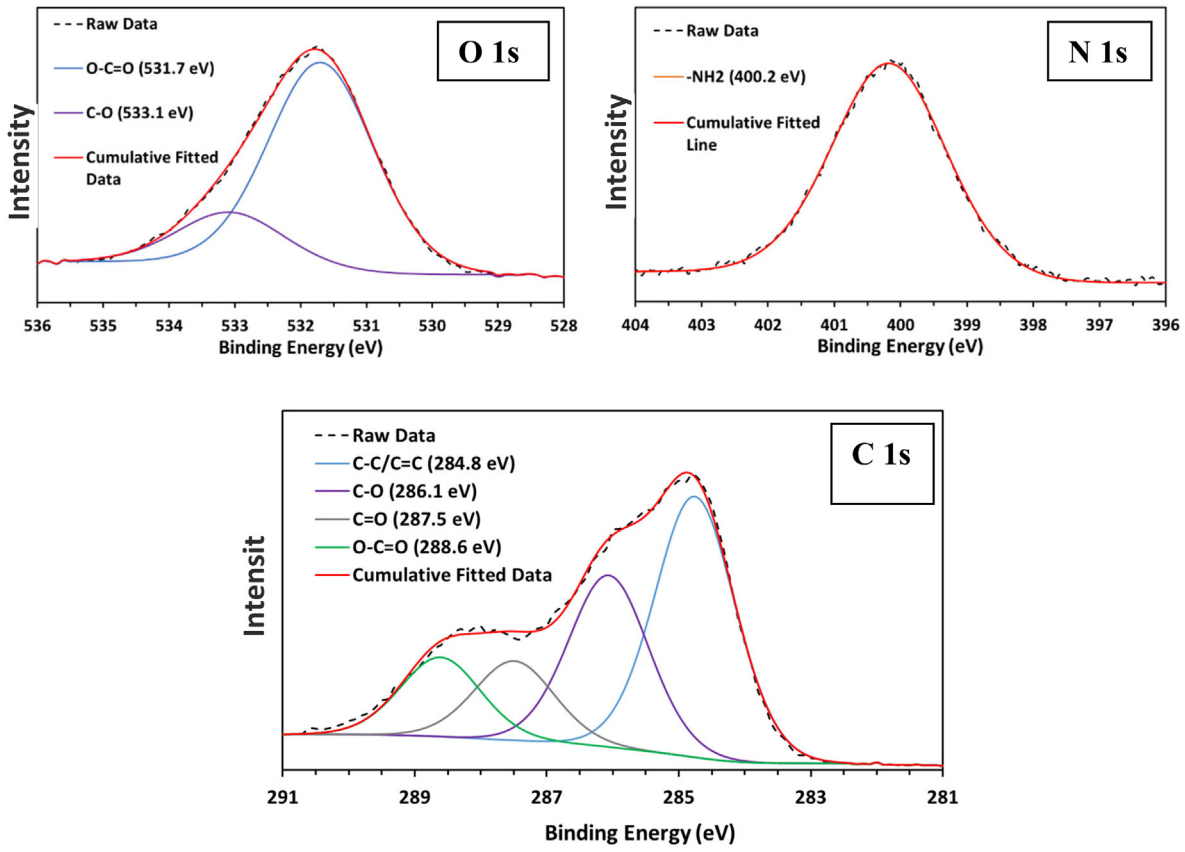

Fig. 4. Deconvoluted high-resolution XPS spectra of F-CDs for O 1 s, N 1 s and C 1 s electrons.

modeled as a continuum dielectric medium with a cavity to accommodate the solute molecule (Robles et al., 2011; Cossi et al., 2003). The XRD patterns and FT-IR spectra reveal graphitic features and substantial disorder. This suggests the nanoparticles to be formed by small planar and curved graphitic flakes connected in such a way that the nanoparticles are compact and approximately spherical, as those also obtained by other synthesis methods (Gutiérrez-García et al., 2019; Ambriz-Torres et al., 2019). To study the functionalization of the carbon nanoparticles by OH and other groups detected in the FT-IR spectra (Fig. 1) we have modeled the nanoparticles by the C_{60} fullerene. Since the hybridization of the C atoms in C_{60} is sp^2, somehow perturbed by the curvature of the surface, the model is expected to retain the main features of the carbon nanoparticle surface relevant for the interaction with the functional groups.

To investigate the interaction of CDs with OH, NH_2 and COOH groups, the structure of the clean CDs was first optimized. Then the functionalization with OH, NH_2 and COOH was separately studied by placing the molecule on different in equivalent positions of the external surface of the CD and relaxing the structure of the system in each case until a local energy minimum was found. The absolute energy minimum corresponds to the most stable adsorption position of the molecule. When OH, COOH and NH_2 are adsorbed at the same time, their locations on the surface

Table 1
Stability period of different nanofluids reported in the literature. The stabilization method and the nanoparticle concentration (in wt%) are given in each case.

Ref	Nanofluid	Stabilization method	Stability	Ref	Nanofluid	Stabilization method	Stability
Asadi et al. (2018)	Al_2O_3-MWCNTs&oil	Ultrasonic waves for 1 h (0.1–1.5 wt%)	7 days	Nabil et al. (2017)	SiO_2-TiO_2 & Water-EG (3 wt%)	Ultrasonic waves for 1.5 h	30 days
Wei et al. (2017)	SiC-TiO_2&oil	Ultrasonic waves for 12 h (0.2–0.8 wt%)	10 days	Yarmand et al. (2016)	GNPs-Pt & Water (0.1 w%)	Functionalization by acid treatment	22 days
Mechiri et al. (2017)	Cu-Zn& oil	Ultrasonic waves for 3 h (0.5 wt%)	3 days	Hamid et al. (2018)	TiO_2-SiO_2 & Water-EG (1wt%)	Ultrasonic waves for 2 h	14 days
Sundar et al. (2014)	MWCNTs-Fe_2O_3&Water	Ultrasonic waves for 1 h (0.3 wt%)	60 days	Sundar et al. (2015)	CNTs-Fe_3O_4 & Water (0.3 wt%)	Ultrasonic waves for 1 h	60 days
Qing et al. (2017)	SiO_2-graphene&oil	Ultrasonic waves for 4 h-pH: 10 (0.04 wt%)	14 days	Esfe et al. (2017)	MWCNTs-ZnO & Water-EG (1 wt%)	Ultrasonic waves for 3 h	10 days
Esfe et al. (2015)	Cu-TiO_2&Water-EG	Ultrasonic waves for 6 h (1.5 wt%)	7 days	Islam et al. (2003)	SWCNT & Water (0.01 wt%)	SDS surfactant and ultrasonic waves for 24 h	90 days
Parsian and Akbari (2018)	Al_2O_3-Cu&EG	Ultrasonic waves for 7 h (2 wt%)	3 days	Kim et al. (2008)	CNT & Water (0.3 wt%)	NaDDBS, CTAB, and Triton X-100 surfactants	>1 day
	Current work	Chemically functionalized (0.5 wt%)	More than a year				

Table 2
Binding energies of OH, COOH and NH_2 groups to CDs.

System	$E_{binding}$ (kJ/mol)
OH@CD	−172.09
COOH@CD	−166.60
NH_2@CD	−149.45
(OH+COOH+NH_2)@CD	−448.57

of the CD have been optimized under the condition that the three functional groups stay far from each other. The adsorption binding energies for each/all functional group(s), given in Table 2, have been calculated according to the following equation (Lim et al., 2016; Seif et al., 2017):

$$E_b = E_{CD\text{-}X(orX3)} - (E_{CD} + E_{X(orX3)}) \quad (4)$$

where $E_{CD\text{-}X}$ represents the total energy for OH, COOH or NH_2 functionalized-CD, and E_{CD} and E_X refer to the energies of CD and each isolated functional group, respectively. The negative sign of the energies in Table 2 indicates that the adsorption is stable. Notice that the X3 notation in Eq. (4) means that all the OH, COOH and NH_2 functional groups have been simultaneously adsorbed. The most stable adsorption configurations are shown in Fig. 6. In the three cases the adsorbed functional group is attached to a C atom. In the case of COOH, its C atom forms a bond with one of the C atoms of the CD substrate. In the other two cases (OH and NH_2), O–C and N–C bonds are formed, respectively. The adsorption binding energies of the OH, NH_2 and COOH groups, shown in Table 2, are between 149 and 172 kJ/mol, a magnitude which reveals the formation of covalent bonds. When the three groups are adsorbed at the same time, they have been placed well separated from each other. The total adsorption energy of 448.6 kJ/mol is only slightly smaller than the sum of the three independent adsorption energies, 488.1 kJ/mol. The formation of covalent bonds supports the experimental observation of these adsorbed groups in the FT-IR spectra, and the observation of carbon, oxygen and nitrogen on the surface of the nanoparticles (Fig. 2S).

Then we have investigated the interaction of the water and ethylene glycol ($C_2H_6O_2$) solvents with clean CDs and with the functionalized particle, (OH+COOH+NH_2)@CD. The optimized structures obtained are given in Fig. 6 for water and Fig. 7 for ethylene glycol, and the corresponding interaction energies

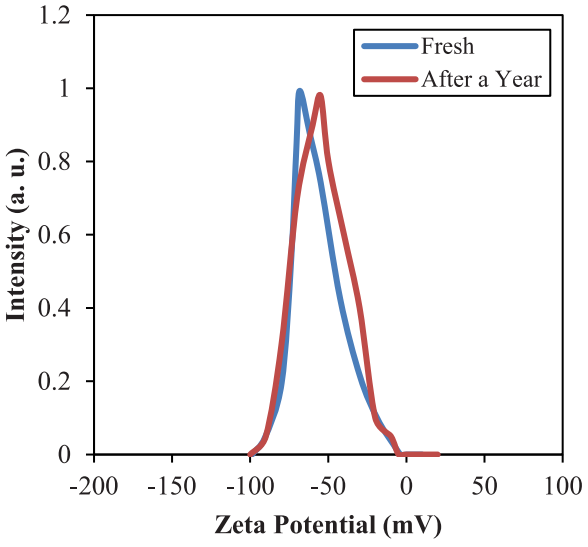

Fig. 5. Zeta potential measurement of F-CDs nanofluid (0.5 Wt%): fresh and after a year.. (For interpretation of the references to color in this figure legend, the reader is referred to the web version of this article.)

are reported in Table 3. The adsorption energies of H_2O and $C_2H_6O_2$ on clean CD are quite weak, −12.57 and −17.63 kJ/mol, respectively. In fact, about ten times smaller than the adsorption energies of the OH, COOH and NH_2 groups on CD. The reason is that covalent bonds (C–O, C–C, C–N) are formed between CD and the OH, COOH and NH_2 groups; instead, water and ethylene glycol sit at larger distances bonded to the fullerene surface by weak dispersion forces.

Three different cases have been considered for the interaction of water and ethylene glycol with the functionalized particle: the water or ethylene glycol molecules interacting with the OH, COOH and NH_2 groups. To find the most stable configuration of each complex (corresponding to the most negative binding energy), several different orientations of the water and ethylene glycol molecules with respect to the functional groups adsorbed on the CD have been considered. The results for the most stable configurations obtained are shown in Fig. 6 for water and Fig. 7 for ethylene glycol. The binding energies of water and ethylene

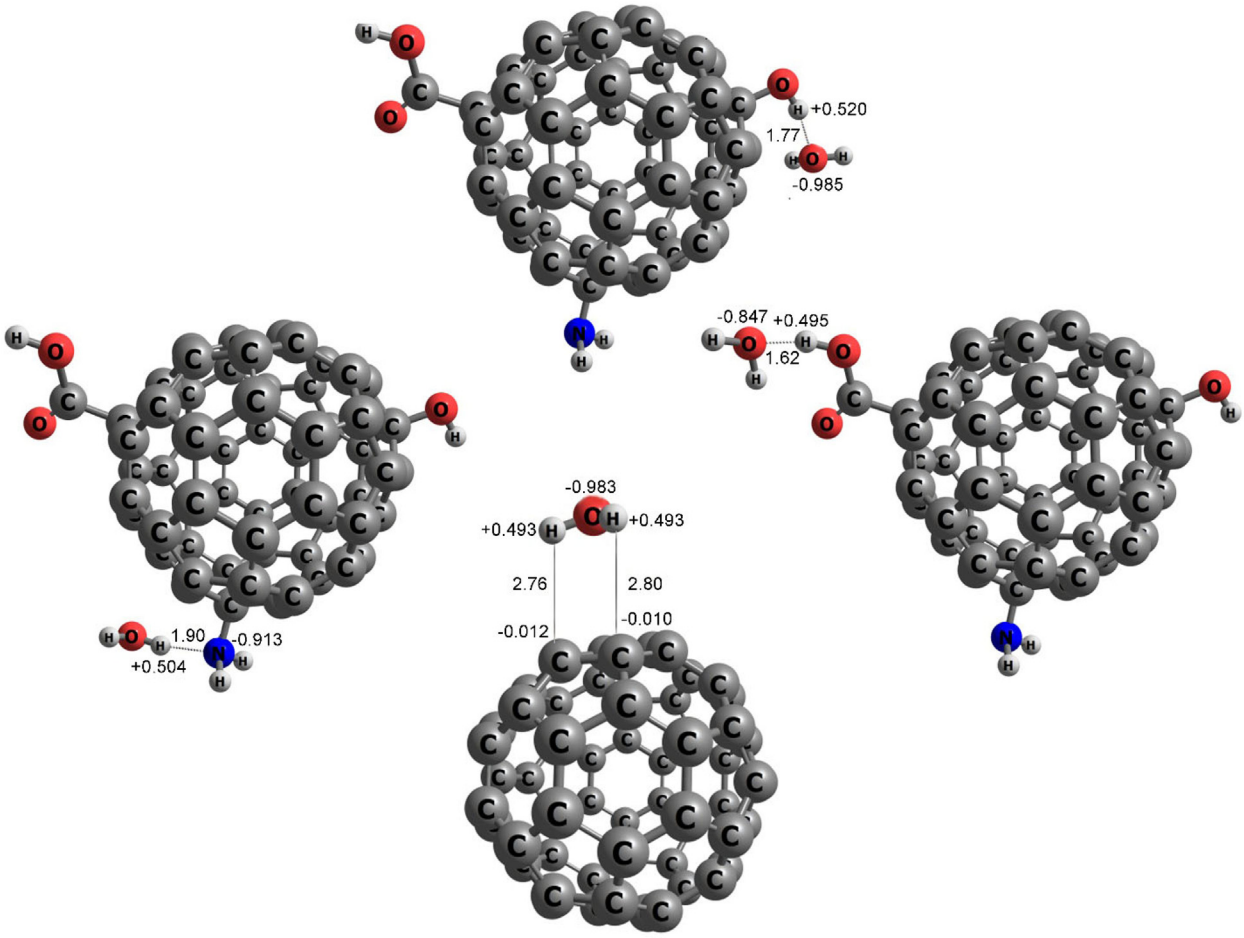

Fig. 6. The most stable configurations for H_2O interacting with the OH, NH_2 and COOH groups of (OH+COOH+NH_2)@CD, and with clean CD. Some relevant bond lengths (in Å) and atomic NBO (natural bond orbitals) charges (in fractions of an electron) are indicated. Negative (positive) charge indicates that the atom has an excess (defect) of electrons. Dark gray, red and blue spheres represent C, O and N atoms, respectively. Small light gray spheres represent H atoms.. (For interpretation of the references to color in this figure legend, the reader is referred to the web version of this article.)

Table 3
Binding energies of water and ethylene glycol (EG) to F-CD (CD functionalized with OH, COOH and NH_2). The functional groups interacting with water or EG are indicated in the second column. Binding energies on clean CD are given for comparison. Charge transfers (CT) between the water or ethylene glycol molecule and F-CD are also reported. Positive (negative) signs of CT indicate that the water or ethylene glycol molecules have a net positive (negative) electric charge, that is, a defect (excess) of electrons.

System	Specific interaction	$E_{binding}$ (kJ/mol)	CT (e)
F-CD-H_2O	H_2O-OH	−75.82	0.048
F-CD-H_2O	H_2O-COOH	−49.96	0.075
F-CD-H_2O	H_2O-NH_2	−31.6	−0.036
CD-H_2O		−12.57	0.003
F-CD-EG	EG-OH	−79.91	0.045
F-CD-EG	EG-COOH	−44.79	0.070
F-CD-EG	EG-NH_2	−41.51	−0.045
CD-EG		−17.63	0.006

glycol on the F-CD have been calculated using the following equation (Cabria et al., 2008; Alemi et al., 2021):

$$E_b = E_{F\text{-}CD/S} - (E_{F\text{-}CD} + E_S) \quad (5)$$

where $E_{F\text{-}CD}$ and E_S are the energies of the functionalized nanoparticle and the isolated H_2O or ethylene glycol solvent molecules (labeled as S), respectively, and $E_{F\text{-}CD/S}$ represents the total energy of the system formed by H_2O or EG adsorbed on F-CD.

The O atom of the water molecule binds to the H atom of the OH and COOH groups, but the interaction with NH_2 is different: one of the H atoms of the water molecule binds to the N atom. The binding energies of the water molecule to the OH, COOH and NH_2 groups functionalizing the carbon particle are larger (more negative) compared to the case of the clean CD, and the intensity of the interaction increases from NH_2 to COOH and then to OH. The trends for the interaction with ethylene glycol are quite similar. One of the O atoms of ethylene glycol binds to the H atom of OH and COOH, and the N atom of NH_2 forms a bond with one of the H atoms of ethylene glycol. The binding energies of ethylene glycol show the same trend as water, and the values are in a similar range. It is clear from the results that the hydroxyl groups, in both cases, provide stronger interactions with the solvent molecules than the COOH and NH_2 groups. The bond lengths d(O–H) of the new intermolecular O–H bonds formed between water or ethylene glycol with the OH group are practically the same, d(O–H) = 1.77–1.78 Å, and this also occurs for the interaction between water or ethylene glycol with the COOH group, with d(O–H) = 1.62 Å in both cases.

Net electronic charge transfers between water or ethylene glycol and the clean or functionalized CD are given in Table 3. A positive (negative) value indicates that the water or ethylene glycol molecules have a net positive (negative) electric charge, that is, a defect (excess) of electrons. The results are in line with the experimental data from Zeta potential. In all cases the net charge transfer is quite small, less than 0.08 electrons, and

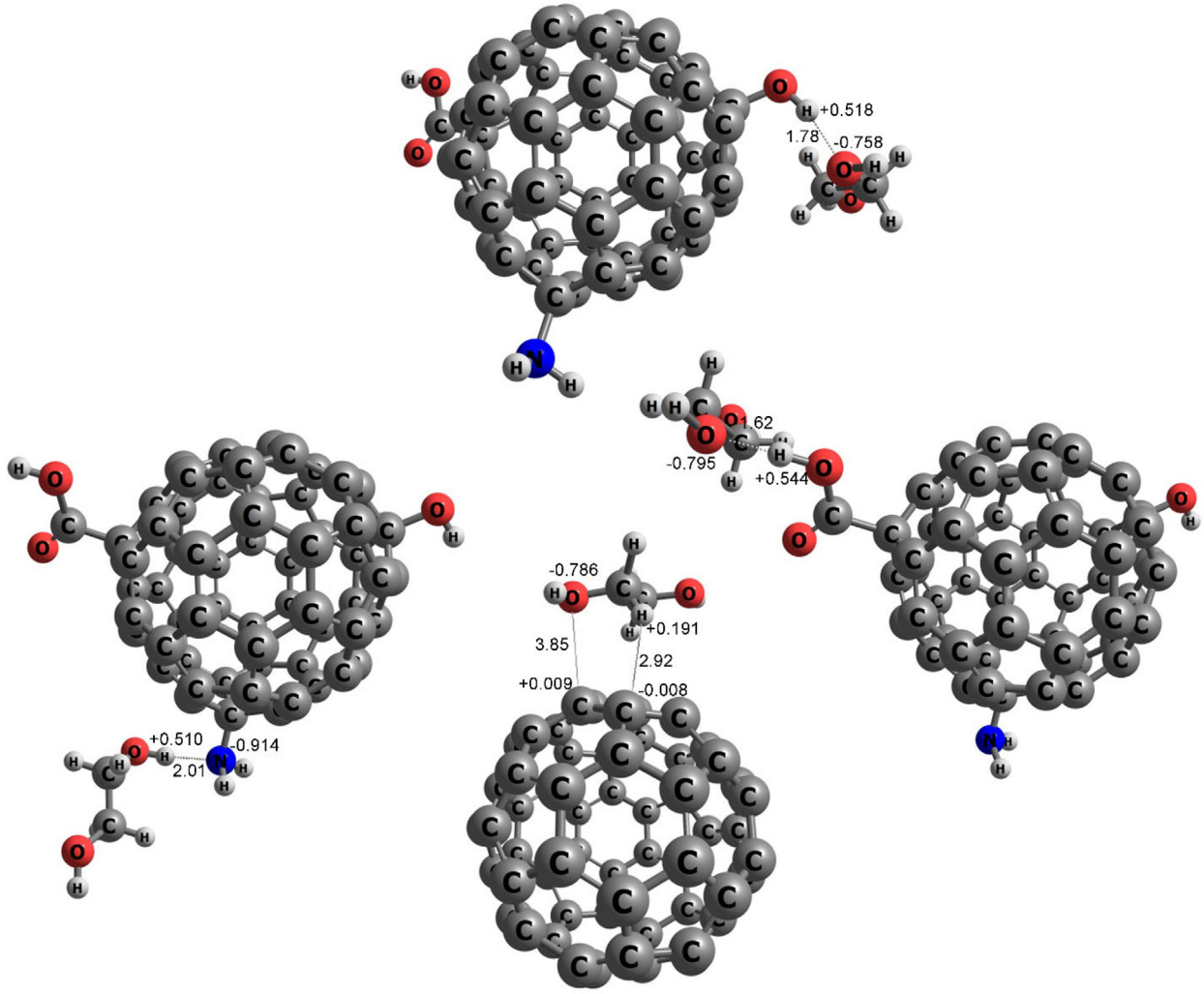

Fig. 7. The most stable configurations for ethylene glycol interacting with the OH, NH_2 and COOH groups of (OH+COOH+NH_2)@CD, and also with clean CD. Some relevant bond lengths (in Å) and atomic NBO (natural bond orbitals) charges (in fractions of an electron) are indicated. Negative (positive) charge indicates that the atom has an excess (defect) of electrons. Dark gray, red and blue spheres represent C, O and N atoms, respectively. Small light gray spheres represent H atoms.. (For interpretation of the references to color in this figure legend, the reader is referred to the web version of this article.)

negligible for bare CDs. However, the charges inside the functional groups and solvent molecules are substantially polarized. In particular, the charges on the specific atoms responsible for the interaction between the functional groups and water or ethylene glycol are large and reveal the contribution to binding through the formation of hydrogen bonds. In addition, since water and ethylene glycol are polar molecules their electric dipoles interact with the dipoles of the OH, COOH and NH_2 groups. These effects become reflected in the interaction energies with water and ethylene glycol given in Table 3, which are substantially higher for functionalized CDs as compared to the non-functionalized CDs. The increased interaction enhances the solubility of the functionalized carbon particles in water and ethylene glycol. Since the solvent used in the experimental work is a mixture of water and ethylene glycol (7:3 ratio), the conclusion is that the functionalization of the carbon nanoparticles with NH_2, OH and COOH significantly enhances their solubility in the water-ethylene glycol fluid. The enhanced solubility prevents the agglomeration of carbon nanoparticles and promotes the long-term stability of the nanofluid, as shown in Fig. 3S and Fig. 5. In addition, when the surfaces of the carbon nanoparticles are substantially covered by NH_2, OH and COOH, agglomeration is prevented by the steric (or protective) effect of those groups. The fact that the most external region of the functionalized particles contains H atoms (see Figs. 6 and 7) also contributes to this protective effect. The calculations indicate that those H atoms are positively charged, with charges close to +0.5 |e|, and those external shells of positive charges also protect the carbon nanoparticles from agglomerating.

3.4. Viscosity and density measurements

Viscosity of fluids is one of the most important factors which can increase the pumping pressure drop and cause increase energy usage (Poongavanam et al., 2019). Thus, in the current work, the viscosity of the nanofluids was investigated as a function of temperature in the range of 20–80 °C and concentration of particles in the range of 0.05–0.5 Wt%, see Fig. 8. The viscosity decreases exponentially with increasing temperature, and in all cases, nanofluids have higher viscosity than the base fluid (water/ethylene glycol; 7:3). Increasing the temperature counteracts the intermolecular forces, which facilitates the fluid moving more easily (Mishra et al., 2014). As can be seen, the viscosity increases as the nanoparticle's concentration increases; hence, the highest viscosity was obtained at the highest particle concentration (0.5 Wt%). For example, the viscosity increased from 1.751 to 1.836 cP as particle concentration increased from 0.05 to 0.5 Wt% at 25 °C. On the other hand, the viscosity decreased as temperature

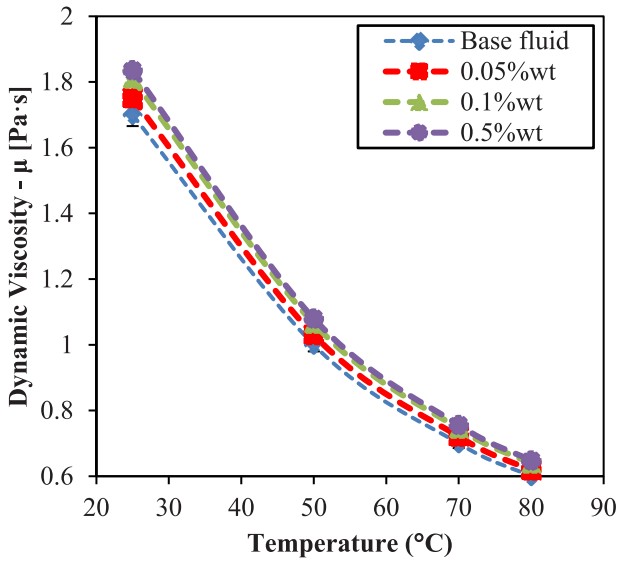

Fig. 8. Variation of dynamic viscosity as a function of nanoparticle concentration and temperature.

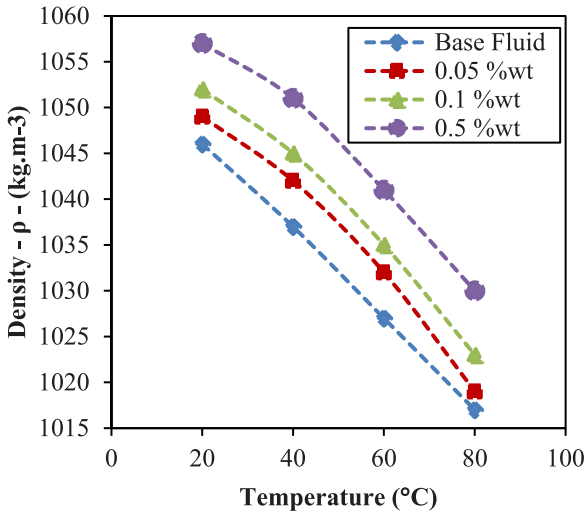

Fig. 9. Variation of nanofluid density as function of particle concentration and temperature.

was raised. By increasing the temperature from 25 to 80 °C, the viscosity decreased from 1.836 to 0.648 cP at concentration of 0.5 Wt%. Increasing temperature enhances the kinetic energy of both nanoparticles and fluid's molecules, counteracting the intermolecular forces; thus, a fluid with more chaotic motion will result. In this condition, both nanoparticles and fluid's molecules move easily; thus, the tendency to flow increases. Dispersing nanoparticles in the base fluid causes an increase of intermolecular adhesion forces; consequently, the tendency to flow decreases compared to the base fluid.

Newtonian and non-Newtonian behavior of nanofluids was investigated by measuring viscosity at different shear rates. Generally, the constant-rate variation of viscosity as a function of shear rate shows the Newtonian behavior of fluids. As seen in Fig. 4S (a), the base fluid and the prepared nanofluids exhibit Newtonian behavior, even at high nanoparticle concentration. And Fig.4S (b) reveals a linear relationship between shear stress and shear rate for the base fluid and nanofluids which confirms the Newtonian behavior.

The density of the nanofluids has a strong impact on the Reynolds number, pressure drop, and friction factor; hence, it is an important property to analyze. The density was investigated as a function of temperature and nanoparticle concentration. Fig. 9 presents the experimental data in the temperature range of 20–80 °C and mass fraction of 0.05–0.5 Wt%. As displayed, increasing temperature has an inverse impact on the density. This is the usual thermal effect; that is, the volume of a given mass of a liquid increases by heating the liquid.

In comparison with the base fluid, nanofluids have higher densities; especially, at higher concentrations, since the solid nanoparticles have higher mass density than the base fluid. However, the nanofluid's density increment is very small even at the highest concentration. To illustrate this point, at a temperature of 60 °C the density of the base fluid is 1027 kg m^{-3}, and increases to 1041 kg m^{-3} at nanoparticle concentration of 0.5 Wt%. In conclusion, although dispersing F-CD nanoparticles in the base fluid caused an increase of density in all range of temperatures and concentrations, the density increment is very small even at the highest concentration, in which case the maximum increment was just 1.2%; thus, it cannot be considered as a limiting factor.

3.5. Thermal performance

To evaluate heat transfer properties of nanofluids, thermal conductivity is one of the factors, which measure heat transfer improvement. In this regard, the KD2 Pro thermal properties analyzer was applied to probe the thermal conductivity of the prepared nanofluids as a function of temperature (25–45 °C) and nanoparticle concentration (0.05–0.5%Wt). As illustrated in Fig. 10, the nanofluids have higher thermal conductivities compared to the base fluid for all the temperatures and concentrations studied. The obtained results revealed that the thermal conductivity enhancement has a direct relationship with temperature. One of the most important reasons is the Brownian motion effect, whose intensity increases at higher temperatures; therefore, the energy transfer increases in the nanofluids, which results in enhanced thermal conductivity. In general, suspended nanoparticles substantially enhance the effective thermal conductivity because the ratio of surface to volume is high in comparison with suspension of micron-size solid particles. To illustrate this point, the highest thermal conductivity enhancement was achieved at concentration of 0.5 Wt% and was equal to 14.28% and 21% at temperatures of 25 °C and 45 °C, respectively. In general, nanoparticles have higher thermal conductivity than the base fluid, and also they tend to experience Brownian motion and cause more turbulency. In addition, nanoparticles make an interconnected thermal bridge that causes transfer heat with a higher speed.

There are numerous investigations in the literature on the performance of nanofluids as heat transfer fluids, and the results are summarized in Table 4. In comparison to these, the current nanofluid which has been prepared with F-CDs nanoparticles fits in the group of fluids having good thermal conductivity; in addition, the facile production method enhances its chance to be employed in an industrial scale to enhance heat transfer and minimize energy usage.

Another important factor to evaluate heat transfer performance of fluids is the convection heat transfer coefficient. It is worth mentioning that, to calculate this coefficient, all thermophysical properties, which were measured in the previous section, are considered. The convection heat transfer coefficient was investigated as a function of Reynolds number and nanoparticle concentration. Since the convection heat transfer coefficient

Table 4
Enhancement in thermal conductivity of various nanofluids reported in the literature.

Reference	Nanofluid	Thermal conductivity enhancement	Reference	Nanofluid	Thermal conductivity enhancement
Esfe et al. (2016)	CNTs-Al_2O_3&water	18% at 34 °C	Munkhbayar et al. (2013)	Silver-MWCNT& water	17% at 50 °C
Harandi et al. (2016)	FMWCNTs-Fe_3O_4&EG	30% at 50 °C	Leong et al. (2010)	CuO&EG	3.8% at 70–95 °C
Esfe et al. (2019)	SWCNTs-MgO&EG	35% at 50 °C	Akhgar and Toghraie (2018)	TiO_2–MWCNT&EG-water	38.7 at 40 °C
Yarmand et al. (2016)	Graphene-Platinum&water	17.77% at 40 °C	Devireddy et al. (2016)	TiO_2&EG-water	4% at 40 °C
Ranjbarzadeh et al. (2019)	Silica&water	38.2% at 55 °C	Zheng et al. (2020)	Fe_3O_4-liquid paraffin	28.49 at 90 °C
Megatif et al. (2016)	TiO_2-CNTs&water	20.5% at 25 °C	Chiam et al. (2017)	Al_2O_3&EG-water	12.8% at 30 °C
Moradi et al. (2020)	TiO_2-MWCNTs&EG-water	34.31% at 60 °C	Esfahani et al. (2018)	ZnO–Ag& water	25% at 50 °C
Ahammed et al. (2016)	Graphene-Alumina&water	13.84% at 50 °C	Oliveira et al. (2017)	MWCNTs-Ag&water	14% at 40 °C
Ouikhalfan et al. (2020)	TiO_2& water	15% at 25 °C		**Current Work**	**21% at 45 °C**

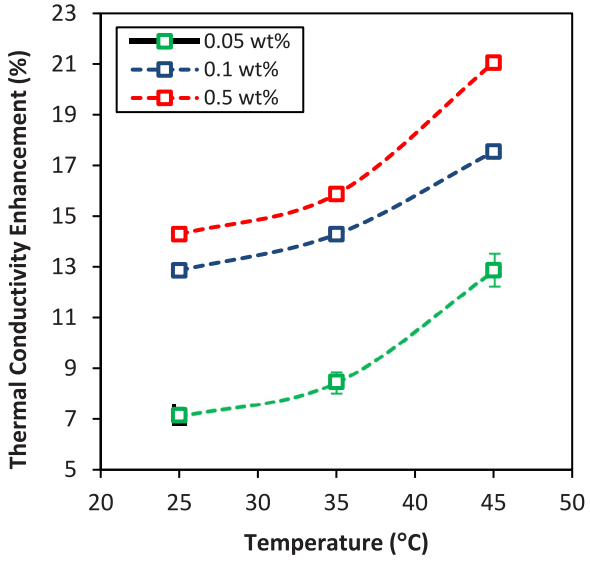

Fig. 10. Thermal conductivity enhancement (%) as a function of particle concentration and temperature (°C).

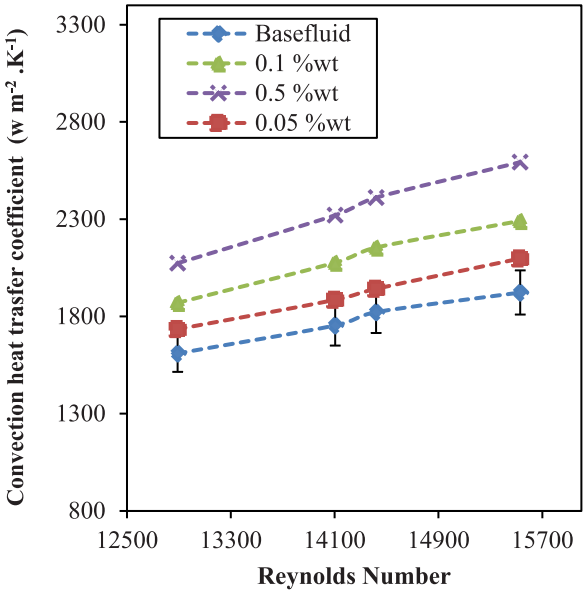

Fig. 11. Convection heat transfer coefficient versus Reynolds number and nanoparticle concentration.

was evaluated by an experimental designed setup, the validation and accuracy of the obtained data is very important. In this regard, we validated the obtained data by comparison with theoretical results which can be found in the reference (Askari et al., 2017). The results obtained for the convection heat transfer coefficient are shown in Fig. 11. It can be seen that increasing nanoparticle concentration and Reynolds number leads to increasing the convection coefficient of heat transfer. Choosing a proper nanoparticle and mass fraction is very important to enhance heat transfer, since in some cases dispersing nanoparticles in fluids may sharply increase the viscosity, which can suppress the heat transfer enhancement (Mikkola et al., 2018; Garg et al., 2009). The results of Fig. 11 illustrate the fact that dispersed nanoparticles noticeably improve heat transfer performance compared to the base fluid in all cases. For example, at concentration of 0.5 Wt% the enhancement is 15 and 34% at Reynolds numbers of 6824 and 15 529, respectively. Moreover, all the results indicate a remarkable enhancement of the convection heat transfer with increasing Reynolds number. While the mass fraction of F-CD nanoparticles increased from 0.05 to 0.5 Wt%, for instance, the ratio of convection heat transfer of nanofluid to the base fluid increased from 1.065 to 1.32 at Reynolds number of 14 419. In general, there are several factors which cause changes in the convection heat transfer compared to the base fluid, such as the Brownian force, friction force between nanoparticles and base fluid, gravity force, Brownian diffusion, dispersion, and sedimentation. Since the suspended nanoparticles are in random movement, they can significantly increase the rate of energy exchange throughout the fluid layers. Consequently, these random motions cause a decrease in the temperature gradient among the fluid layers. Overall, the enhancement of heat transfer by nanofluids can mainly be understood as due to two main reasons: The first one is that the dispersed nanoparticles enhance the thermal conductivity of the fluid; the second one is that the energy exchange among the fluid layers is enhanced due to chaotic movement of the nanoparticles.

4. Conclusions

In this work, a thorough experimental investigation of thermophysical properties of ultra-stable nanofluids is reported. A simple hydrothermal method was applied to synthesize carbon nanoparticles functionalized with OH, COOH and NH_2 groups. The presence of oxygen and nitrogen within the carbon framework led to a highly hydrophilic surface of the synthesized nanoparticles, resulting in high dispersibility in polar and protic media and

formation of stable nanofluids. The ultra-stability of nanofluids prepared by dispersing the functionalized carbon nanoparticles into a mixture of water and ethylene glycol was confirmed by Zeta potential analysis (−61.5 mV), showing that the prepared nanofluid remained stable even after a year. Furthermore, the long-term stability of the nanofluid was supported by DFT calculations. Interestingly, the role that the functional groups attached to the surface of the nanoparticles play in enhancing the stability of the nanofluid was clearly observed. The improved solubility arises from the hydrogen bonds and electrostatic dipolar interactions between the functionalized nanoparticles and the base fluid. Thermo-physical properties of the nanofluids including viscosity, density, and thermal conductivity were evaluated at different temperatures (20–45 °C) and nanoparticle concentrations (0.05–0.5 Wt%). The viscosity measurements proved that dispersing nanoparticles in the base fluid caused a viscosity increase in all ranges of temperature and concentration. The maximum viscosity increase (8%) occurred at 0.5 Wt% and 20 °C. In addition, the nanofluid showed a Newtonian behavior in all ranges of nanoparticle concentration and temperature. The measurements showed that the density is not a limiting factor because the maximum density increase was 1.2% compared to the base fluid. As for the thermal conductivity, an increasing trend has been observed as the temperature and nanoparticle concentration increases, the maximum enhancement was approximately 21% at 45 °C and 0.5 Wt%. Besides, in comparison with the base fluid, the synthesized nanofluid showed a remarkable increase of the convective heat transfer coefficient over all Reynolds number ranges. The maximum enhancement was 34% at the Reynolds number of 15 529 and nanoparticle concentration of 0.5 Wt%.

CRediT authorship contribution statement

Saeed Askari: Data curation, Methodology, Investigation, Writing - review & editing. **Ehsanollah Ettefaghi:** Data curation, Investigation. **Alimorad Rashidi:** Conceptualization, Investigation, Methodology, Supervision, Writing - review & editing. **Abdolvahab Seif:** Conceptualization, Investigation, Methodology, Software, Writing - review & editing, Validation. **Jennifer A. Rudd:** Data curation, Writing - review & editing. **Julio A. Alonso:** Conceptualization, Investigation, Methodology, Writing - review & editing, Validation. **Saeed Khodabakhshi:** Data curation, Writing - review & editing.

Declaration of competing interest

The authors declare that they have no known competing financial interests or personal relationships that could have appeared to influence the work reported in this paper.

Acknowledgments

Support of this work by Iran Research Institute of Petroleum Industry (RIPI) is gratefully acknowledged. Saeid Khodabakhshi wishes to acknowledge funding from the European Union's Horizon 2020 Research and Innovation Program under the Marie Skłodowska-Curie grant agreement No 663830. The work of JAA was supported by Junta de Castilla y León, Spain (Grant VA021G18), Ministerio de Ciencia e Innovación of Spain (Project PID2019104924RBI00), and University of Valladolid (GIR Nanostructure Physics), Spain.

Appendix A. Supplementary data

Supplementary material related to this article can be found online at https://doi.org/10.1016/j.egyr.2021.07.001.

References

Ahammed, N., Asirvatham, L.G., Wongwises, S., 2016. Entropy generation analysis of graphene–alumina hybrid nanofluid in multiport minichannel heat exchanger coupled with thermoelectric cooler. Int. J. Heat Mass Transfer 103, 1084–1097.

Akhgar, A., Toghraie, D., 2018. An experimental study on the stability and thermal conductivity of water-ethylene glycol/TiO2-MWCNTs hybrid nanofluid: developing a new correlation. Powder Technol. 338, 806–818.

Akram, Naveed, Montazer, Elham, Kazi, S.N., M.Soudagar, Manzoore Elahi, Ahmed, Waqar, Mohd Zubir, Mohd Nashrul, et al., 2021. Experimental investigations of the performance of a flat-plate solar collector using carbon and metal oxides based nanofluids. Energy 227, 120452.

Alemi, F.M., Mohammadi, S., Dehghani, S.A.M., Rashidi, A., Hosseinpour, N., Seif, A., 2021. Experimental and DFT studies on the effect of carbon nanoparticles on asphaltene precipitation and aggregation phenomena. Chem. Eng. J. 422, 130030.

Ambreen, T., Kim, M.-H., 2020. Influence of particle size on the effective thermal conductivity of nanofluids: A critical review. Appl. Energy 264, 114684.

Ambriz-Torres, J., Gutiérrez-García, C., Contreras-Navarrete, J., Granados-Martínez, F., García-Ruiz, D., Flores-Ramírez, N., et al., 2019. Synthesis and characterization of carbon spheres/poly (methyl methacrylate) composites with enhanced electrical conductivity and vickers microhardness. J. Electron. Mater. 1–8.

Asadi, A., Asadi, M., Rezaniakolaei, A., Rosendahl, L.A., Afrand, M., Wongwises, S., 2018. Heat transfer efficiency of Al2O3-MWCNT/thermal oil hybrid nanofluid as a cooling fluid in thermal and energy management applications: An experimental and theoretical investigation. Int. J. Heat Mass Transfer 117, 474–486.

Ashraf, K., Siddique, I., Hussain, A., 2020. Impact of thermophoresis and brownian motion on non-Newtonian nanofluid flow with viscous dissipation near stagnation point. Phys. Scr. 95, 055217.

Askari, S., Koolivand, H., Pourkhalil, M., Lotfi, R., Rashidi, A., 2017. Investigation of Fe3O4/graphene nanohybrid heat transfer properties: Experimental approach. Int. Commun. Heat Mass Transfer 87, 30–39.

Bazmi, M., Askari, S., Ghasemy, E., Rashidi, A., Ettefaghi, E., 2019. Nitrogen-doped carbon nanotubes for heat transfer applications. J. Thermal Anal. Calorimetry 138, 69–79.

Borode, A., Ahmed, N., Olubambi, P., 2019. A review of solar collectors using carbon-based nanofluids. J. Cleaner Prod. 118311.

Cabria, I., López, M., Alonso, J., 2008. Hydrogen storage capacities of nanoporous carbon calculated by density functional and Møller-Plesset methods. Phys. Rev. B 78, 075415.

Chiam, H., Azmi, W., Usri, N., Mamat, R., Adam, N., 2017. Thermal conductivity and viscosity of Al2O3 nanofluids for different based ratio of water and ethylene glycol mixture. Exp. Therm Fluid Sci. 81, 420–429.

Choudhary, R., Khurana, D., Kumar, A., Subudhi, S., 2017. Stability analysis of al2o3/water nanofluids. J. Exp. Nanosci. 12, 140–151.

Cossi, M., Rega, N., Scalmani, G., Barone, V., 2003. Energies, structures, and electronic properties of molecules in solution with the C-PCM solvation model. J. Comput. Chem. 24, 669–681.

Devireddy, S., Mekala, C.S.R., Veeredhi, V.R., 2016. Improving the cooling performance of automobile radiator with ethylene glycol water based tio2 nanofluids. Int. Commun. Heat Mass Transfer 78, 121–126.

Ding, H., Cheng, L.-W., Ma, Y.-Y., Kong, J.-L., Xiong, H.-M., 2013. Luminescent carbon quantum dots and their application in cell imaging. New J. Chem. 37, 2515–2520.

Esfahani, N.N., Toghraie, D., Afrand, M., 2018. A new correlation for predicting the thermal conductivity of ZnO–Ag (50%–50%)/water hybrid nanofluid: an experimental study. Powder Technol. 323, 367–373.

Esfe, M.H., Esfandeh, S., Amiri, M.K., Afrand, M., 2019. A novel applicable experimental study on the thermal behavior of SWCNTs (60%)-MgO (40%)/EG hybrid nanofluid by focusing on the thermal conductivity. Powder Technol. 342, 998–1007.

Esfe, M.H., Esfandeh, S., Saedodin, S., Rostamian. Experimental evaluation, H., 2017. Sensitivity analyzation and ANN modeling of thermal conductivity of ZnO-MWCNT/EG-water hybrid nanofluid for engineering applications. Appl. Therm. Eng. 125, 673–685.

Esfe, M.H., Saedodin, S., Yan, W.-M., Afrand, M., Sina, N., 2016. Study on thermal conductivity of water-based nanofluids with hybrid suspensions of CNTs/Al 2 O 3 nanoparticles. J. Thermal Anal. Calorimetry 124, 455–460.

Esfe, M.H., Wongwises, S., Naderi, A., Asadi, A., Safaei, M.R., Rostamian, H., et al., 2015. Thermal conductivity of Cu/TiO2–water/EG hybrid nanofluid: Experimental data and modeling using artificial neural network and correlation. Int. Commun. Heat Mass Transfer 66, 100–104.

Esmaeili, E., Rounaghi, S.A., Gruner, W., Eckert, J., 2019. The preparation of surfactant-free highly dispersed ethylene glycol-based aluminum nitride-carbon nanofluids for heat transfer application. Adv. Powder Technol..

Frisch, M., Trucks, G., Schlegel, H., Scuseria, G., Robb, M., Cheeseman, J., et al., 2010. Gaussian 09. Revis. C 01, Gaussian Inc. Wallingford, CT. (2009).

Garg, P., Alvarado, J.L., Marsh, C., Carlson, T.A., Kessler, D.A., Annamalai, K., 2009. An experimental study on the effect of ultrasonication on viscosity and heat transfer performance of multi-wall carbon nanotube-based aqueous nanofluids. Int. J. Heat Mass Transfer 52, 5090–5101.

Gupta, M., Singh, V., Kumar, S., Kumar, S., Dilbaghi, N., Said, Z., 2018. Up to date review on the synthesis and thermophysical properties of hybrid nanofluids. J. Cleaner Prod. 190, 169–192.

Gutiérrez-García, C.J., Ambriz-Torres, J.M., de Jesús Contreras-Navarrete, J., Granados-Martínez, F.G., García-Ruiz, D.L., García-González, L., et al., 2019. Synthesis of carbon spheres by atmospheric pressure chemical vapor deposition from a serial of aromatic hydrocarbon precursors. Physica E 112, 78–85.

Hamid, K.A., Azmi, W., Nabil, M., Mamat, R., 2018. Experimental investigation of nanoparticle mixture ratios on TiO2–SiO2 nanofluids heat transfer performance under turbulent flow. Int. J. Heat Mass Transfer 118, 617–627.

Harandi, S.S., Karimipour, A., Afrand, M., Akbari, M., D'Orazio, A., 2016. An experimental study on thermal conductivity of F-MWCNTs–Fe3O4/EG hybrid nanofluid: effects of temperature and concentration. Int. Commun. Heat Mass Transfer 76, 171–177.

Hussein, O.A., Habib, K., Muhsan, A.S., Saidur, R., Alawi, O.A., Ibrahim, T.K., 2020. Thermal performance enhancement of a flat plate solar collector using hybrid nanofluid. Sol. Energy 204, 208–222.

Islam, M., Rojas, E., Bergey, D., Johnson, A., Yodh, A., 2003. High weight fraction surfactant solubilization of single-wall carbon nanotubes in water. Nano Lett. 3, 269–273.

Jiang, Z., Palacios, A., Lei, X., Navarro, M., Qiao, G., Mura, E., et al., 2019. Novel key parameter for eutectic nitrates based nanofluids selection for concentrating solar power (CSP) systems. Appl. Energy 235, 529–542.

Jóźwiak, B., Dzido, G., Zorębski, E., Kolanowska, A., Jędrysiak, R., Dziadosz, J., et al., 2020. Remarkable thermal conductivity enhancement in carbon-based ionanofluids: Effect of nanoparticle morphology. ACS Appl. Mater. Interfaces 12, 38113–38123.

Karthikeyan, A., Coulombe, S., Kietzig, A., Stein, R.S., van de Ven, T., 2018. Interaction of oxygen functionalized multi-walled carbon nanotube nanofluids with copper. Carbon 140, 201–209.

Kazemi, Iman, Sefid, Mohammad, Masoud, Afrand, 2020. Improving the thermal conductivity of water by adding mono & hybrid nano-additives containing graphene and silica: A comparative experimental study. Int. Commun. Heat Mass Transfer 116, 104648.

Kim, H.-S., Park, W.-I., Kang, M., Jin, H.-J., 2008. Multiple light scattering measurement and stability analysis of aqueous carbon nanotube dispersions. J. Phys. Chem. Solids 69, 1209–1212.

Kumar, P.M., Palanisamy, K., Vijayan, V., 2019. Stability analysis of heat transfer hybrid/water nanofluids. In: Materials Today: Proceedings.

Leong, K., Saidur, R., Kazi, S., Mamun, A., 2010. Performance investigation of an automotive car radiator operated with nanofluid-based coolants (nanofluid as a coolant in a radiator). Appl. Therm. Eng. 30, 2685–2692.

Li, Xiaoke, Chen, Wenjing, Zou, Changjun, 2020b. The stability, viscosity and thermal conductivity of carbon nanotubes nanofluids with high particle concentration: A surface modification approach. Powder Technol. 361, 957–967.

Li, X., Guan, B.Y., Gao, S., Lou, X.W.D., 2019. A general dual-templating approach to biomass-derived hierarchically porous heteroatom-doped carbon materials for enhanced electrocatalytic oxygen reduction. Energy Environ. Sci. 12, 648–655.

Li, W., Wang, Y., Zou. Stability, C., 2020a. Thermal conductivity and supercooling behavior of novel β-CD-TiO2-Ag cooling medium-based nanofluids for eco-friendly cold thermal energy storage. J. Cleaner Prod. 121162.

Lim, G., Lee, K.B., Ham, H.C., 2016. Effect of N-containing functional groups on CO2 adsorption of carbonaceous materials: a density functional theory approach. J. Phys. Chem. C 120, 8087–8095.

Lyu, B., Li, H.-J., Xue, F., Sai, L., Gui, B., Qian, D., et al., 2020. Facile, gram-scale and eco-friendly synthesis of multi-color graphene quantum dots by thermal-driven advanced oxidation process. Chem. Eng. J. 124285.

Mechiri, S., Vasu, V., Venu Gopal, A., 2017. Investigation of thermal conductivity and rheological properties of vegetable oil based hybrid nanofluids containing Cu–Zn hybrid nanoparticles. Exp. Heat Transfer 30, 205–217.

Megatif, L., Ghozatloo, A., Arimi, A., Shariati-Niasar, M., 2016. Investigation of laminar convective heat transfer of a novel TiO2–carbon nanotube hybrid water-based nanofluid. Exp. Heat Transfer 29, 124–138.

Mikkola, V., Puupponen, S., Granbohm, H., Saari, K., Ala-Nissila, T., Seppälä, A., 2018. Influence of particle properties on convective heat transfer of nanofluids. Int. J. Therm. Sci. 124, 187–195.

Minkowycz, W., Sparrow, E., Abraham, J.P., 2016. Nanoparticle Heat Transfer and Fluid Flow. CRC Press.

Mishra, P.C., Mukherjee, S., Nayak, S.K., Panda, A., 2014. A brief review on viscosity of nanofluids. Int. Nano Lett. 4, 109–120.

Mondal, T.K., Saha, S.K., 2019. Facile approach to synthesize nitrogen-and oxygen-rich carbon quantum dots for pH sensor, fluorescent indicator, and invisible ink applications. ACS Sustain. Chem. Eng. 7, 19669–19678.

Moradi, A., Zareh, M., Afrand, M., Khayat, M., 2020. Effects of temperature and volume concentration on thermal conductivity of TiO2-MWCNTs (70-30)/EG-water hybrid nano-fluid. Powder Technol. 362, 578–585.

Mori, S., Mt Aznam, S., Yanagisawa, R., Yokomatsu, F., Okuyama, K., 2019. Measurement of a heated surface temperature using a high-speed infrared camera during critical heat flux enhancement by a honeycomb porous plate in a saturated pool boiling of a nanofluid. Heat Transfer Eng. 1–17.

Mukherjee, S., Mishra, P.C., Chaudhuri, P., 2018. Stability of heat transfer nanofluids – a review. Chem. Bio. Eng. Rev. 5, 312–333.

Munkhbayar, B., Tanshen, M.R., Jeoun, J., Chung, H., Jeong, H., 2013. Surfactant-free dispersion of silver nanoparticles into MWCNT-aqueous nanofluids prepared by one-step technique and their thermal characteristics. Ceram. Int. 39, 6415–6425.

Nabil, M., Azmi, W., Hamid, K.A., Mamat, R., Hagos, F.Y., 2017. An experimental study on the thermal conductivity and dynamic viscosity of TiO2-SiO2 nanofluids in water: ethylene glycol mixture. Int. Commun. Heat Mass Transfer 86, 181–189.

Nojoomizadeh, M., Karimipour, A., Firouzi, M., Afrand, M., 2018. Investigation of permeability and porosity effects on the slip velocity and convection heat transfer rate of Fe3O4/water nanofluid flow in a microchannel while its lower half filled by a porous medium. Int. J. Heat Mass Transfer 119, 891–906.

Oliveira, G.A., Contreras, E.M.C., Bandarra Filho, E.P., 2017. Experimental study on the heat transfer of MWCNT/water nanofluid flowing in a car radiator. Appl. Therm. Eng. 111, 1450–1456.

Ouikhalfan, M., Labihi, A., Belaqziz, M., Chehouani, H., Benhamou, B., Sarı, A., et al., 2020. Stability and thermal conductivity enhancement of aqueous nanofluid based on surfactant-modified tio2. J. Dispersion Sci. Technol. 41, 374–382.

Park, S.J., Park, J.Y., Chung, J.W., Yang, H.K., Moon, B.K., Yi, S.S., 2020. Color tunable carbon quantum dots from wasted paper by different solvents for anti-counterfeiting and fluorescent flexible film. Chem. Eng. J. 383, 123200.

Parsian, A., Akbari, M., 2018. New experimental correlation for the thermal conductivity of ethylene glycol containing al 2 o 3–cu hybrid nanoparticles. J. Thermal Anal. Calorimetry 131, 1605–1613.

Poongavanam, G.K., Panchabikesan, K., Murugesan, R., Duraisamy, S., Ramalingam, V., 2019. Experimental investigation on heat transfer and pressure drop of MWCNT-Solar glycol based nanofluids in shot peened double pipe heat exchanger. Powder Technol. 345, 815–824.

Pourreza, A., Askari, S., Rashidi, A., Seif, A., Kooti, M., 2019. Highly efficient SO3Ag-functionalized MIL-101 (Cr) for adsorptive desulfurization of the gas stream: Experimental and DFT study. Chem. Eng. J. 363, 73–83.

Qeays, I.A., Yahya, S.M., Asjad, M., Khan, Z.A., 2020. Multi-performance optimization of nanofluid cooled hybrid photovoltaic thermal system using fuzzy integrated methodology. J. Cleaner Prod. 256, 120451.

Qing, S.H., Rashmi, W., Khalid, M., Gupta, T., Nabipoor, M., Hajibeigy, M.T., 2017. Thermal conductivity and electrical properties of hybrid SiO2-graphene naphthenic mineral oil nanofluid as potential transformer oil. Mater. Res. Exp. 4, 015504.

Ranjbarzadeh, R., Moradikazerouni, A., Bakhtiari, R., Asadi, A., Afrand, M., 2019. An experimental study on stability and thermal conductivity of water/silica nanofluid: Eco-friendly production of nanoparticles. J. Cleaner Prod. 206, 1089–1100.

Robles, J., López, M., Alonso, J., 2011. Modeling of the functionalization of single-wall carbon nanotubes towards its solubilization in an aqueous medium. Eur. Phys. J. D 61, 381–388.

Sarsam, W.S., Kazi, S., Badarudin, A., 2015. A review of studies on using nanofluids in flat-plate solar collectors. Sol. Energy 122, 1245–1265.

Seif, A., López, M., Granja-DelRío, A., Azizi, K., Alonso, J., 2017. Adsorption and growth of palladium clusters on graphdiyne. Phys. Chem. Chem. Phys. 19, 19094–19102.

Sert, Y., Balakit, A.A., Öztürk, N., Ucun, F., El-Hiti, G.A., 2014. Experimental (FT-IR, NMR and UV) and theoretical (M06-2X and DFT) investigation, and frequency estimation analyses on (E)-3-(4-bromo-5-methylthiophen-2-yl) acrylonitrile. Spectrochim. Acta Part A: Mol. Biomol. Spectrosc. 131, 502–511.

Sharma, S., Mehta, S., Ibhadon, A., Kansal, S., 2019. Fabrication of novel carbon quantum dots modified bismuth oxide (α-Bi2O3/C-dots): Material properties and catalytic applications. J. Colloid Interface Sci. 533, 227–237.

Shdaifat, A., Yacoub, M., Zulkifli, R., Sopian, K., Salih, A.A., 2020. Thermal and hydraulic performance of cuo/water nanofluids: a review. Micromachines 11, 416.

Sözen, A., Ç. Filiz, Aytac, I., Martin, K., Ali, H.M., Boran, K., et al., 2021. Upgrading of the performance of an air-to-air heat exchanger using graphene/water nanofluid. Int. J. Thermophys. 42, 1–15.

Srivastava, R., Al-Omary, F.A., El-Emam, A.A., Pathak, S.K., Karabacak, M., Narayan, V., et al., 2017. A combined experimental and theoretical DFT (B3LYP, CAM-B3LYP and M06-2X) study on electronic structure, hydrogen bonding, solvent effects and spectral features of methyl 1H-indol-5-carboxylate. J. Mol. Struct. 1137, 725–741.

Sundar, L.S., Singh, M.K., Sousa, A.C., 2014. Enhanced heat transfer and friction factor of MWCNT–Fe3O4/water hybrid nanofluids. Int. Commun. Heat Mass Transfer 52, 73–83.

Sundar, L.S., Sousa, A.C., Singh, M.K., 2015. Heat transfer enhancement of low volume concentration of carbon nanotube-Fe3O4/water hybrid nanofluids in a tube with twisted tape inserts under turbulent flow. J. Thermal Sci. Eng. Appl. 7, 021015.

Tehrani, N.H.M.H., Alivand, M.S., Maklavany, D.M., Rashidi, A., Samipoorgiri, M., Seif, A., et al., 2019. Novel asphaltene-derived nanoporous carbon with NS-rich micro-mesoporous structure for superior gas adsorption: Experimental and DFT study. Chem. Eng. J. 358, 1126–1138.

Wang, Q., Wang, Z.-B., Li, R., Liu, H., Yang, M., Li, C., et al., 2018. Flower-like nitrogen-oxygen-doped carbon encapsulating sulfur composite synthesized via in-situ oxidation approach. Chem. Eng. J. 345, 271–279.

Wei, B., Zou, C., Yuan, X., Li, X., 2017. Thermo-physical property evaluation of diathermic oil based hybrid nanofluids for heat transfer applications. Int. J. Heat Mass Transfer 107, 281–287.

Wong, K.V., De Leon, O., 2017. Applications of Nanofluids: Current and Future. Nanotechnology and Energy. Jenny Stanford Publishing, pp. 105–132.

Yarmand, H., Gharehkhani, S., Shirazi, S.F.S., Goodarzi, M., Amiri, A., Sarsam, W.S., et al., 2016. Study of synthesis, stability and thermo-physical properties of graphene nanoplatelet/platinum hybrid nanofluid. Int. Commun. Heat Mass Transfer 77, 15–21.

Zhang, Z., Zhang, J., Chen, N., Qu, L., 2012. Graphene quantum dots: an emerging material for energy-related applications and beyond. Energy Environ. Sci. 5, 8869–8890.

Zhao, Y., Schultz, N.E., Truhlar, D.G., 2006. Design of density functionals by combining the method of constraint satisfaction with parametrization for thermochemistry, thermochemical kinetics, and noncovalent interactions. J. Chem. Theory Comput. 2, 364–382.

Zhao, Y., Truhlar, D.G., 2008. The M06 suite of density functionals for main group thermochemistry, thermochemical kinetics, noncovalent interactions, excited states, and transition elements: two new functionals and systematic testing of four M06-class functionals and 12 other functionals. Theor. Chem. Accounts 120, 215–241.

Zheng, Y., Shahsavar, A., Afrand, M., 2020. Sonication time efficacy on fe3o4-liquid paraffin magnetic nanofluid thermal conductivity: an experimental evaluation. Ultras. Sonochem. 105004.